

Computing phase diagrams for a quasicrystal-forming patchy-particle system

Aleks Reinhardt, Flavio Romano, and Jonathan P. K. Doye*
Physical and Theoretical Chemistry Laboratory, Department of Chemistry,
University of Oxford, Oxford, OX1 3QZ, United Kingdom
(Dated: 8 April 2013)

We introduce an approach to computing the free energy of quasicrystals, which we use to calculate phase diagrams for systems of two-dimensional patchy particles with five regularly arranged patches that have previously been shown to form dodecagonal quasicrystals. We find that the quasicrystal is a thermodynamically stable phase for a wide range of conditions and remains a robust feature of the system as the potential's parameters are varied. We also demonstrate that the quasicrystal is entropically stabilised over its crystalline approximants.

Quasicrystals are a type of aperiodic crystal structure: they have well-ordered structures, but cannot be described by a periodic lattice, not even one with incommensurate lattice parameters [1]. They were first reported by Shechtman *et al.* [2], in whose work a rapidly cooled Al-Mn alloy was found to result in a metastable quasicrystal. Most quasicrystals discovered so far are metallic alloys [1]; however, recently, an increasing number of examples have been reported in the field of soft condensed matter [3]. Quasicrystals have also been observed to form in computer simulations, in which not only binary, but also one-component quasicrystals have been seen [4–8]. While certain quasicrystals have been shown to be stable in experiment [9], in simulations, the relatively short timescales accessible mean that it is not necessarily clear whether quasicrystals are truly the stable phase, or rather a metastable phase that is more kinetically accessible. In this work, we address this important question of assessing the stability of quasicrystals and apply it to a soft matter system that has the potential to be realised experimentally.

To prove that quasicrystals are thermodynamically stable, their free energy must be computed. However, such a calculation is not straightforward: the principal problem is that there is no obvious reference state whose free energy is known and from which thermodynamic integration [10, 11] could be used to calculate the free energy of the quasicrystalline phase. A phase transition intervenes when integrating from an ideal gas, which is normally used as a reference state for fluid phases, and an Einstein crystal, used as a reference state for crystalline phases, would also not be suitable because it would fail to capture the configurational entropy associated with the quasicrystal's many possible structures.

One approach to assessing quasicrystal stability is to compute the free energy of an approximant crystalline phase. However, it is not immediately obvious whether quasicrystals are more or less stable than their approximants [5, 6]; whilst the enthalpy and vibrational properties of the quasicrystal and its approximant phases are likely to be similar, the free energy of a quasicrystal has a contribution from its configurational entropy that is not present for the approximant [7]. Nevertheless, such calculations have provided some insight into the phase behaviour of systems such as hard tetrahedra and bipyramids [6] and spherical micelles [7]. By contrast, Kiselev *et al.* recently estimated the free energy of the quasicrystal itself by combining a phonon contribution for a particular quasicrystal configuration from thermodynamic integration and a configura-

tional contribution based on an approximation of uncorrelated phason flips [12]. They confirmed that, within their approximation, the quasicrystal's free energy is in certain conditions lower than the approximant's.

Our solution to this conundrum is to note that thermodynamic integration is not the only way the melting point of a solid can be computed. Another method is to simulate the direct coexistence of two phases with an interface [10]. By performing such simulations at a range of temperatures, we can bracket the regions where the quasicrystal melts ($T > T_{\text{fus}}$) and grows ($T < T_{\text{fus}}$). At $T = T_{\text{fus}}$, the chemical potential of the quasicrystal is equal to that of the fluid, which we can calculate using thermodynamic integration. Such an equilibrium approach by construction accounts for the quasicrystal's configurational entropy. Once the quasicrystal's free energy is known at one point, we can use thermodynamic integration to reach other points of interest on the phase diagram.

Here, we apply this approach to a two-dimensional system of patchy particles [13] with five regularly arranged attractive patches, which we model using a simple potential that has previously been used in simulations of self-assembly and crystallisation [8, 14–16]. The potential is based on the Lennard-Jones (LJ) form, $V^{\text{LJ}}(r_{ij}) = 4\epsilon[(\sigma_{\text{LJ}}/r_{ij})^{2n} - (\sigma_{\text{LJ}}/r_{ij})^n]$, where $n = 6$ for the standard LJ potential, where for $r_{ij} > \sigma_{\text{LJ}}$, this potential is multiplied by an angular modulation factor

$$V^{\text{A}} = \exp\left[\frac{-\theta_{k_{\text{min}ij}^2}}{2\sigma_{\text{pw}}^2}\right] \exp\left[\frac{-\theta_{l_{\text{min}ji}^2}}{2\sigma_{\text{pw}}^2}\right], \quad (1)$$

where σ_{pw} is the 'patch width' (in radians) and θ_{kij} is the angle between the patch vector of patch k (chosen to minimise this angle) on particle i and the interparticle vector r_{ij} .

This interaction potential provides a simple model for the patchy colloidal particles that many experimental groups have, with progressively increasing success, been seeking to develop [13, 17, 18]. The enhanced range of structural behaviour that such patchy interactions could facilitate has been extensively studied in computer simulation [8, 14–16, 19].

Dodecagonal quasicrystals were previously found to form on cooling systems of these five-patch particles in certain conditions, and structures with the lowest enthalpy were also identified [8]. Some of the relevant phases studied are shown in Fig. 1(a–d); particles are classified based on a common neighbour analysis [8] into σ , H and Z environments (shown in Fig. 1(e)), by analogy to the Frank–Kasper phases [20]. The

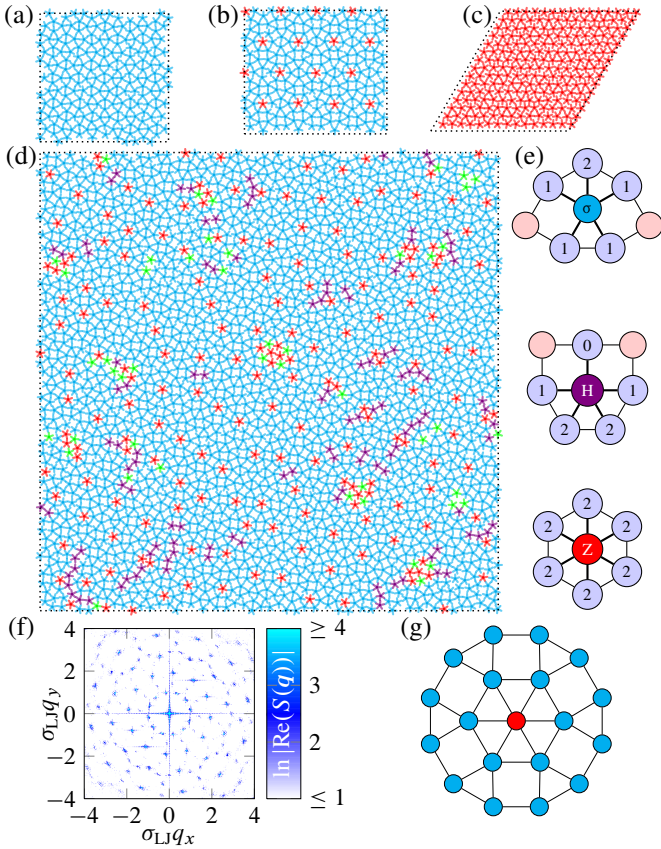


FIG. 1. Examples of the main phases studied. (a) σ phase. (b) Approximant crystal. (c) Plastic hexagonal (Z) phase. (d) Quasicrystal, $N = 2500$. (e) Neighbour classification of σ , H and Z environments. The numbers of common neighbours are given for each of the central particle's neighbours. These local environments are used to colour the particles in (a)–(d), where in addition, particles that do not adopt one of these environments are coloured green. (e) Diffraction pattern corresponding to the configuration shown in (a). (f) Dodecagonal motif characteristic of the quasicrystal.

hexagonal (Z) phase (Fig. 1(c)) was found to form at high pressures (as it is densest) and for wide patches (where the potential is closer to being isotropic). At low pressures and at reasonably narrow patch widths, the structure best satisfying the attractive patches is the enthalpically favoured phase. A crystal cannot exist with five-fold symmetry, and so no crystal with five perfectly aligned patches exists. As a compromise, each particle has five neighbours, but the angles between the neighbours do not perfectly match the five-fold symmetry of the particle itself. Local environments satisfying this requirement are the σ and H environments shown in Fig. 1(e); the lowest enthalpy structure at low pressure and reasonably narrow patch widths is the σ crystal shown in Fig. 1(a) [8].

Quasicrystals were observed in some cooling runs in the region where the σ phase is the lowest in enthalpy, but near to the hexagonal ‘boundary’. The structure of a typical quasicrystal is shown in Fig. 1(d); its diffraction pattern (Fig. 1(f)) exhibits a characteristic twelve-fold symmetry. The local environments in the quasicrystal are predominantly of the σ type, but a significant fraction of Z environments can be seen: these are typically

located at the centre of a dodecagonal motif (Fig. 1(g)). Much of the structure can be analysed in terms of packing of such dodecagons into triangular, square and rectangular arrangements [8], which can readily be seen in Fig. 1(d); the various possible ways of arranging these dodecagons are likely to lead to substantial entropy. There is no translational order, but bonds can be orientated in any one of twelve directions, resulting in long-range orientational order of dodecagonal character.

We perform Monte Carlo simulations in the NpT ensemble using a rectangular box with periodic boundaries [21]. As a starting point in the determination of phase diagrams for this system, we chose a patch width, temperature and pressure at which the quasicrystal is known to form on cooling, and thus locate the fluid-quasicrystal (F-QC) equilibrium transition. This transition is mostly rapid and facile, with essentially no hysteresis, which allows us to determine the coexistence points directly by performing simulations in relatively large boxes starting from both phases. Whilst we initially performed direct coexistence simulations to determine the melting point of the quasicrystal, these simulations mostly did not prove to be any more efficient than direct brute-force simulations, in which no initial interface was introduced, as the growth of the phases was not restricted to the initial interface. This lack of hysteresis is most likely indicative of a particularly low F-QC interfacial free energy. Phase transitions can be observed from a kink in the potential energy or density plotted against the variable we are changing (such as the temperature or the pressure). However, we can further test for the nature of the phase by calculating appropriate diffraction patterns: the quasicrystal exhibits a distinctive 12-fold diffraction pattern (Fig. 1(f)), the Z phase exhibits a six-fold pattern, and the fluid phase does not exhibit a well-defined pattern.

Once a F-QC coexistence point is known, we can equate the chemical potential of the fluid (as calculated by thermodynamic integration) with that of the quasicrystal. From here, we can use thermodynamic integration to calculate the chemical potential of the quasicrystal at other temperatures and pressures. By also performing thermodynamic integration to find the chemical potential of the σ phase, we can locate the putative σ -QC transition. We plot in Fig. 2 the free energies of the σ , QC and F phases as a function of T at a constant $p/k_B T$. From this figure, we can identify two clear transitions (σ -QC and QC-F), and a temperature window in which the quasicrystal is thermodynamically stable. In the same figure, we also show the free energy of an approximant crystal phase that is based on the most common packing of dodecagons in the quasicrystal; it is never thermodynamically stable. To rationalise why the quasicrystal is stable, we also calculate the enthalpy (obtained directly from simulations) and hence obtain the entropy as a function of the temperature. These functions are also depicted in Fig. 2, and it is clear that in the region in which the quasicrystal is stable, it does indeed have a higher enthalpy than the σ phase, but its significantly higher entropy nevertheless allows it to become more stable. The origin of this entropy is a combination of the differing vibrational properties and the configurational disorder present in the quasicrystalline phase. If we assume the vibrational properties of the quasicrystal and

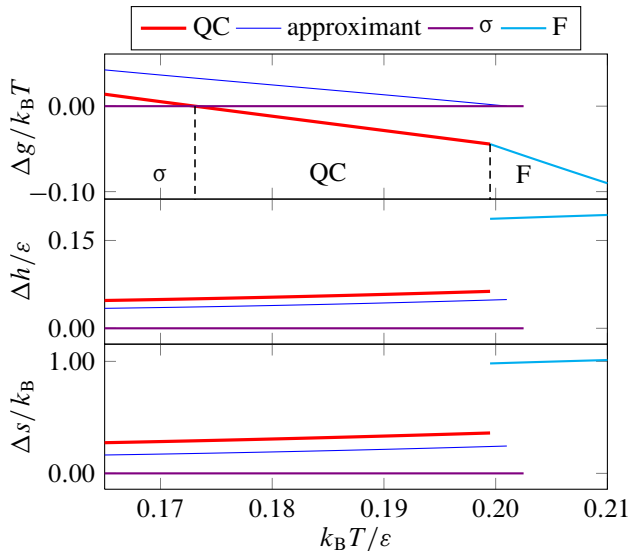


FIG. 2. Per-particle Gibbs energies, enthalpies and entropies, relative to the σ phase, as a function of T at $\sigma_{\text{LJ}}^2 p / k_B T = 1.5$, $\sigma_{\text{pw}} = 0.49$ and $n = 6$. Lines end at the limit of (meta)stability of the phases. Dashed lines denote coexistence points, $k_B T_{\sigma \leftrightarrow \text{QC}} / \epsilon = 0.173$ and $k_B T_{\text{QC} \leftrightarrow \text{F}} / \epsilon = 0.1995$. The stable phase in each region is explicitly marked. The error in $\Delta g / k_B T$ is $< 0.012 k_B T$ [21].

its approximant are identical, the configurational component of this entropy can be estimated from the entropy difference between the quasicrystal and its approximant, $\Delta s / k_B \approx 0.113$ at $T_{\sigma \leftrightarrow \text{QC}}$ [22].

From Fig. 2, we can determine two coexistence points on the phase diagram. We construct the remainder of the phase diagram partly through the same procedure as above at, say, other pressures, but also through the use of Gibbs–Duhem integration [10, 24]. This method allows us to integrate Clapeyron equation analogues to obtain new coexistence points from already known coexistence points, but requires metastability and hysteresis in the transition so that the simulated phases retain their identity when simulated at and around the coexistence point. As a result, the method cannot be applied to the QC-F and QC-Z transitions for much of the phase diagram due to their relative reversibility.

The resulting phase diagram is shown in Fig. 3(a). We note that the quasicrystal is stable for a wide range of pressures. At very high pressures, the Z phase becomes stable due to its greater density. The Z phase is a plastic crystal, meaning that particles are able to rotate relatively freely: this is understandable, as there is no obvious preferred way to orientate a five-fold particle in a six-fold environment [25]. No orientational ordering ensues in the Z phase even at low temperatures. Whether it would form an orientationally-ordered crystal or an orientational glass at sufficiently low T is not clear. It is noteworthy that for the QC-Z transition, $dp/dT < 0$; since $\rho_Z > \rho_{\text{QC}}$, the Clapeyron equation implies that $S_Z > S_{\text{QC}}$: this is likely to stem from the orientational entropy of the plastic crystal. Interestingly, in addition to the two triple points (σ -QC-Z and QC-Z-F), there is a range of pressures where the stable thermodynamic phase changes from F to Z to QC to σ as the system is cooled.

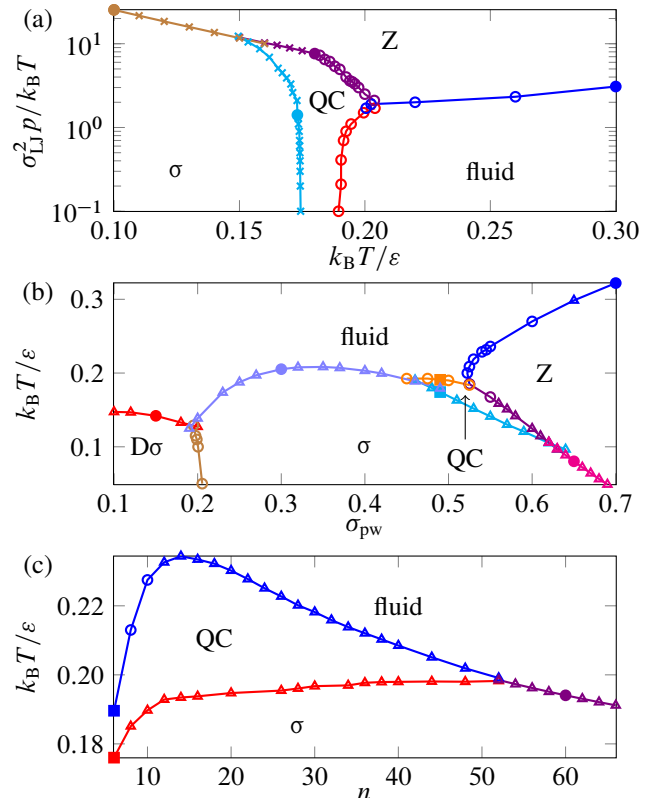


FIG. 3. Phase diagrams. Markers show the technique used to obtain each point: Frenkel–Ladd and thermodynamic integration (filled circles), Gibbs–Duhem integration (crosses), hamiltonian Gibbs–Duhem integration (triangles) and direct simulation (open circles). Points obtained from previous phase diagrams are shown as squares. (a) p/T - T phase diagram; $\sigma_{\text{pw}} = 0.49$, $n = 6$. (b) T - σ_{pw} phase diagram; $\sigma_{\text{LJ}}^2 p / k_B T = 0.5$, $n = 6$. (c) T - n phase diagram; $\sigma_{\text{LJ}}^2 p / k_B T = 0.5$, $\sigma_{\text{pw}} = 0.49$.

We also look at the effect of modifying potential parameters on the phase diagram, thus allowing us to assess the extent of quasicrystal stability and how finely-tuned the particle properties would need to be to observe a quasicrystalline phase in experiment. To determine the phase diagram as the potential parameters change, we additionally use hamiltonian Gibbs–Duhem integration, whereby we numerically integrate a Clapeyron equation that has been generalised to allow for changes to the potential itself [10].

We first investigate the behaviour of the system as the patch width is varied. From the phase diagram in Fig. 3(b), we see that the quasicrystal is only stable for a limited range of σ_{pw} , although the range may perhaps be wider at other pressures. As the patch width narrows, the quasicrystal becomes increasingly enthalpically destabilised with respect to the σ phase, as the many six-fold environments cannot satisfactorily fulfil patch-patch interactions. By contrast, as the patch width increases, the quasicrystal becomes more stable with respect to the σ phase, but the hexagonal phase is stabilised even more: as the patches are wider and closer to the isotropic case, six-fold environments are enthalpically preferred.

Another noteworthy feature of this phase diagram is that below $\sigma_{\text{pw}} \approx 0.35$, $T_{\sigma \leftrightarrow \text{F}}$ begins to decrease: as the patches

become narrower, there is an increasing energetic penalty for patches that do not point directly at each other. For very narrow patches, the σ phase transforms into a distorted σ phase ($D\sigma$) [16], in which three of the five patches point directly at the patches of neighbouring particles, thus breaking the square symmetry of the lattice. The reason for this behaviour is that at narrow patch widths, only ‘perfect’ connections count, as a slight misalignment of the patches rapidly reduces the interparticle attraction, and three perfect interactions become favoured over five imperfect ones.

Because colloidal interactions are often quite short-ranged, we also wish to investigate what happens to the system when we change the LJ exponent (n), which changes the range of the potential and the width of the potential well. We show the phase diagram as a function of n in Fig. 3(c). The effects of increasing n on isotropic potentials are well understood [26]: the liquid phase is energetically destabilised because the intrinsic disorder in interparticle neighbour distances is penalised by the narrower potential [27]. In Fig. 3(c), the range of stability of the quasicrystal initially increases. The enthalpies of the QC and σ phases increase only slightly as n increases, because their relative order means that most interparticle neighbour distances can be close to optimal, but do so more for the quasicrystal, as some disorder is typically present in the quasicrystal configurations (for example, particles with unclassified environments in Fig. 1(d)); the σ -QC coexistence temperature does therefore increase slightly. By contrast, the fluid is initially much more enthalpically penalised: the fluid enthalpy increases rapidly, and the fluid density decreases as n increases. At the maximum in $T_{QC\leftrightarrow F}$ ($n \approx 14$), the size of the temperature window of quasicrystal stability is three times that of the $n = 6$ LJ potential. However, a narrower potential well associated with increasing n also means that there is less vibrational entropy associated with the ordered structures, and beyond $n \approx 14$, this effect becomes dominant. The QC-F coexistence temperature decreases until the quasicrystal loses stability at $n \approx 53$.

The potential at the higher values of n shown in Fig. 3(c) is very short-ranged indeed. The fact that the quasicrystal maintains and even increases its window of stability for ranges of attraction typical of colloidal particles suggests that this is a robust, general result and that stable quasicrystals can be expected to form in experimental realisations of this system.

There are several potential approaches to such experimental realisations. If patchy colloidal particles similar to the ones studied here could be created, it would be reasonable to expect that a quasicrystal may form when they are confined in two dimensions. For example, Chen *et al.* observed the formation of a 2D kagomé lattice from tri-block Janus particles by introducing a density mismatch with the solvent to confine their colloidal system into two dimensions [18]. A possible alternative to using colloidal patchy particles might involve the use of DNA multi-arm motifs [28], for which a variety of 2D crystalline arrays have been observed for motifs with different numbers of arms, including a σ phase for five-arm motifs that is analogous to what we see in the current model when patches are narrow. However, such DNA motifs have a well-defined ‘valence’, and there is no equivalent of the patch width that

could be tuned to make two co-ordination numbers compete. Therefore, a possible approach to forming a DNA quasicrystal might be to use a two-component mixture of five-arm and six-arm motifs of the appropriate composition.

In summary, we have shown how we can compute if and where a quasicrystalline phase is thermodynamically stable. To the best of our knowledge, this is the first such calculation of the chemical potential of a quasicrystal and the associated phase diagrams that has been obtained directly from simulations with no approximations. For our patchy particle system, we found that the quasicrystalline phase is stable over a significant portion of the phase diagram and is stabilised primarily by its configurational entropy. It is robust to parameter changes in the model, which inspires confidence that such a thermodynamically stable quasicrystal might be experimentally realised.

We wish to thank the Engineering and Physical Sciences Research Council for financial support.

* Correspondence author. E-mail: jonathan.doye@chem.ox.ac.uk

REFERENCES

- [1] W. Steurer, *Z. Kristallogr.* **219**, 391 (2004); *Chem. Soc. Rev.* **41**, 6719 (2012).
- [2] D. Shechtman, I. Blech, D. Gratias, and J. W. Cahn, *Phys. Rev. Lett.* **53**, 1951 (1984).
- [3] X. Zeng, *Curr. Opin. Colloid In.* **9**, 384 (2005); S. Fischer, A. Exner, K. Zielske, J. Perlich, S. Deloudi, W. Steurer, P. Lindner, and S. Förster, *Proc. Natl. Acad. Sci. U.S.A.* **108**, 1810 (2011); T. Dotera, *Isr. J. Chem.* **51**, 1197 (2011).
- [4] M. Widom, K. J. Strandburg, and R. H. Swendsen, *Phys. Rev. Lett.* **58**, 706 (1987); P. W. Leung, C. L. Henley, and G. V. Chester, *Phys. Rev. B* **39**, 446 (1989); M. Dzugutov, *Phys. Rev. Lett.* **70**, 2924 (1993); A. Skibinsky, S. V. Buldyrev, A. Scala, S. Havlin, and H. E. Stanley, *Phys. Rev. E* **60**, 2664 (1999); M. Engel and H.-R. Trebin, *Phys. Rev. Lett.* **98**, 225505 (2007); A. S. Keys and S. C. Glotzer, *Phys. Rev. Lett.* **99**, 235503 (2007); J. C. Johnston, S. Phippen, and V. Molinero, *J. Phys. Chem. Lett.* **2**, 384 (2011); J. C. Johnston, N. Kastelowitz, and V. Molinero, *J. Chem. Phys.* **133**, 154516 (2010); C. Zhi-Wei and F. Xiu-Jun, *Chinese Phys. Lett.* **29**, 050204 (2012); T. Dotera, *J. Polym. Sci.: Pol. Phys.* **50**, 155 (2012).
- [5] A. Haji-Akbari, M. Engel, A. S. Keys, X. Zheng, R. G. Petschek, P. Palffy-Muhoray, and S. C. Glotzer, *Nature* **462**, 773 (2009).
- [6] A. Haji-Akbari, M. Engel, and S. C. Glotzer, *Phys. Rev. Lett.* **107**, 215702 (2011); *J. Chem. Phys.* **135**, 194101 (2011).
- [7] C. R. Iacovella, A. S. Keys, and S. C. Glotzer, *Proc. Natl. Acad. Sci. U.S.A.* **108**, 20935 (2011).
- [8] M. N. van der Linden, J. P. K. Doye, and A. A. Louis, *J. Chem. Phys.* **136**, 054904 (2012).
- [9] A.-P. Tsai, *Acc. Chem. Res.* **36**, 31 (2003).
- [10] C. Vega, E. Sanz, J. L. F. Abascal, and E. G. Noya, *J. Phys.: Cond. Matt.* **20**, 153101 (2008).
- [11] D. Frenkel and A. J. C. Ladd, *J. Chem. Phys.* **81**, 3188 (1984).
- [12] A. Kiselev, M. Engel, and H.-R. Trebin, *Phys. Rev. Lett.* **109**, 225502 (2012).
- [13] S. C. Glotzer and M. J. Solomon, *Nat. Mater.* **6**, 557 (2007);

- A. B. Pawar and I. Kretzschmar, *Macromol. Rapid Comm.* **31**, 150 (2010).
- [14] A. W. Wilber, J. P. K. Doye, A. A. Louis, E. G. Noya, M. A. Miller, and P. Wong, *J. Chem. Phys.* **127**, 085106 (2007); E. G. Noya, C. Vega, J. P. K. Doye, and A. A. Louis, *J. Chem. Phys.* **127**, 054501 (2007); *J. Chem. Phys.* **132**, 234511 (2010); A. J. Williamson, A. W. Wilber, J. P. K. Doye, and A. A. Louis, *Soft Matter* **7**, 3423 (2011); G. Doppelbauer, E. G. Noya, E. Bianchi, and G. Kahl, *J. Phys.: Cond. Matt.* **24**, 284124 (2012).
- [15] J. P. K. Doye, A. A. Louis, I. C. Lin, L. R. Allen, E. G. Noya, A. W. Wilber, H. C. Kok, and R. Lyus, *Phys. Chem. Chem. Phys.* **9**, 2197 (2007).
- [16] G. Doppelbauer, E. Bianchi, and G. Kahl, *J. Phys.: Cond. Matt.* **22**, 104105 (2010).
- [17] G. A. DeVries, M. Brunnbauer, Y. Hu, A. M. Jackson, B. Long, B. T. Neltner, O. Uzun, B. H. Wunsch, and F. Stellacci, *Science* **315**, 358 (2007); Y.-S. Cho, G.-R. Yi, S.-H. Kim, S.-J. Jeon, M. T. Elsesser, H. K. Yu, S.-M. Yang, and D. J. Pine, *Chem. Mater.* **19**, 3183 (2007); S.-M. Yang, S.-H. Kim, J.-M. Lim, and G.-R. Yi, *J. Mater. Chem.* **18**, 2177 (2008); D. J. Kraft, W. S. Vlug, C. M. van Kats, A. van Blaaderen, A. Imhof, and W. K. Kegel, *J. Am. Chem. Soc.* **131**, 1182 (2009); L. Wang, L. Xia, G. Li, S. Ravaine, and X. S. Zhao, *Angew. Chem., Int. Ed.* **47**, 4725 (2008); Z. Mao, H. Xu, and D. Wang, *Adv. Funct. Mater.* **20**, 1053 (2010); E. Duguet, A. Desert, A. Perro, and S. Ravaine, *Chem. Soc. Rev.* **40**, 941 (2011); Y. Wang, Y. Wang, D. R. Breed, V. N. Manoharan, L. Feng, A. D. Hollingsworth, M. Weck, and D. J. Pine, *Nature* **491**, 51 (2012).
- [18] Q. Chen, S. C. Bae, and S. Granick, *Nature* **469**, 381 (2011).
- [19] N. Kern and D. Frenkel, *J. Chem. Phys.* **118**, 9882 (2003); Z. Zhang and S. C. Glotzer, *Nano Lett.* **4**, 1407 (2004); E. Bianchi, J. Largo, P. Tartaglia, E. Zaccarelli, and F. Sciortino, *Phys. Rev. Lett.* **97**, 168301 (2006); F. Sciortino, A. Giacometti, and G. Pastore, *Phys. Rev. Lett.* **103**, 237801 (2009); F. Romano and F. Sciortino, *Soft Matter* **7**, 5799 (2011); E. Bianchi, R. Blaak, and C. N. Likos, *Phys. Chem. Chem. Phys.* **13**, 6397 (2011).
- [20] F. C. Frank and J. S. Kasper, *Acta Crystallogr.* **11**, 184 (1958); *Acta Crystallogr.* **12**, 483 (1959).
- [21] See supplementary material in the appendix for implementation details and a summary of simulation methods used.
- [22] This value of Δs is significantly larger than the tiling entropy of a random Stampfli tiling, but somewhat smaller than that of a maximally random square-triangle tiling, where both have been evaluated at zero phason strain [23].
- [23] M. Oxborrow and C. L. Henley, *Phys. Rev. B* **48**, 6966 (1993).
- [24] D. A. Kofke, *Mol. Phys.* **78**, 1331 (1993); *J. Chem. Phys.* **98**, 4149 (1993).
- [25] We have also considered the additional non-plastic hexagonal crystal structures suggested by Doppelbauer *et al.* for pentavalent patchy particles [16], but these were found quickly to lose their rotational specificity at the temperatures used in our simulations.
- [26] M. H. J. Hagen and D. Frenkel, *J. Chem. Phys.* **101**, 4093 (1994); G. A. Vliegenthart, J. F. M. Lodge, and H. N. W. Lekkerkerker, *Physica A* **263**, 378 (1999).
- [27] J. P. K. Doye and D. J. Wales, *Science* **271**, 484 (1996).
- [28] H. Yan, S. H. Park, G. Finkelstein, J. H. Reif, and T. H. LaBean, *Science* **301**, 1882 (2003); Y. He, Y. Chen, H. Liu, A. E. Ribbe, and C. Mao, *J. Am. Chem. Soc.* **127**, 12202 (2005); Y. He, Y. Tian, A. E. Ribbe, and C. Mao, *J. Am. Chem. Soc.* **128**, 15978 (2006); C. Zhang, M. Su, Y. He, X. Zhao, P.-a. Fang, A. E. Ribbe, W. Jiang, and C. Mao, *Proc. Natl. Acad. Sci. U.S.A.* **105**, 10665 (2008).
- [29] N. Metropolis, A. W. Rosenbluth, M. N. Rosenbluth, A. H. Teller, and E. Teller, *J. Chem. Phys.* **21**, 1087 (1953).
- [30] D. Frenkel and B. Smit, *Understanding molecular simulation: From algorithms to applications*, 2nd ed. (Elsevier Academic Press, San Diego, London, 2002).
- [31] R. Eppenga and D. Frenkel, *Mol. Phys.* **52**, 1303 (1984).
- [32] A. J. C. Ladd and L. V. Woodcock, *Chem. Phys. Lett.* **51**, 155 (1977).
- [33] G. T. Gao, X. C. Zeng, and H. Tanaka, *J. Chem. Phys.* **112**, 8534 (2000).

Supplementary material

Simulation details

The simulations described in our work used the Metropolis Monte Carlo approach [29] in the isobaric-isothermal ensemble [30, 31] with periodic boundary conditions.

The potential as discussed in the manuscript is given more formally by

$$V(\mathbf{r}_{ij}, \varphi_i, \varphi_j) = \begin{cases} V^{\text{LJ}}(r_{ij}) & r_{ij} < \sigma_{\text{LJ}}, \\ V^{\text{LJ}}(r_{ij})V^{\text{A}}(\hat{\mathbf{r}}_{ij}, \varphi_i, \varphi_j) & \sigma_{\text{LJ}} \leq r_{ij}, \end{cases} \quad (2)$$

where \mathbf{r}_{ij} is the interparticle vector connecting the centres of the two particles i and j , r_{ij} is its magnitude, φ_i and φ_j are the orientations of the particles i and j , the generalised Lennard-Jones potential is

$$V^{\text{LJ}}(r_{ij}) = 4\epsilon \left[(\sigma_{\text{LJ}}/r_{ij})^{2n} - (\sigma_{\text{LJ}}/r_{ij})^n \right], \quad (3)$$

where $n = 6$ for the standard Lennard-Jones potential, and

$$V^{\text{A}}(\hat{\mathbf{r}}_{ij}, \varphi_i, \varphi_j) = \exp \left[\frac{-\theta_{k_{\min}ij}^2}{2\sigma_{\text{pw}}^2} \right] \exp \left[\frac{-\theta_{\min ji}^2}{2\sigma_{\text{pw}}^2} \right], \quad (4)$$

where σ_{pw} is the patch width, θ_{kij} is the angle between the patch vector of patch k on particle i and the interparticle vector \mathbf{r}_{ij} , and k_{\min} is the patch that minimises the magnitude of this angle. Two particles therefore interact only through a single pair of patches. In the simulations reported here, we use a potential cutoff of $r_{\text{cut}} = 3\sigma_{\text{LJ}}$, and the potential in Eq. (3) is shifted so that it equals zero at $r_{ij} = r_{\text{cut}}$. The crossover to including angular modulation in the potential (Eq. (2)) is likewise adjusted so that it still occurs when the potential energy is identically zero.

Most simulations reported used relatively small system sizes (of the order of 500 particles), but the phase diagram in Fig. 3(a) and the free energies in Fig. 2 were also calculated using a system of the order of 2500 particles, and certain transitions were calculated with systems of 5000 and 10000 particles, with no detectable differences in the behaviour of the systems, confirming that reasonably small simulations were sufficient to calculate phase diagrams.

Summary of methods

Here, we summarise the methods we used in the manuscript in somewhat more detail. The approaches described here are all standard and are provided here as a quick summary for the benefit of the reader only.

Direct coexistence vs brute force simulation

Direct coexistence simulations [10, 32] are simulations in which an explicit interface is set up between the two phases in question, and the thermodynamically stable phase is expected to grow into the thermodynamically unstable phase such that the interface between the two phases moves. In brute force simulations, no interface is set up; instead, a single phase is simulated and it spontaneously converts into the thermodynamically stable phase. Typically, this brute force simulation process is prone to hysteresis effects, where for example the quasicrystal will form at some temperature T_1 , but when the quasicrystal is heated in a reverse brute force simulation, it will melt at temperature T_2 , where $T_2 > T_1$, because nucleation involves a free energy barrier that must be overcome. In direct coexistence simulations, this hysteresis does not occur, because both phases are present from the start, and the interface between them is pre-formed.

In our simulations, we established that there is essentially no hysteresis between the quasicrystal and the fluid under the conditions described in this paragraph, and so direct coexistence simulations offer no advantage over brute force simulations. Indeed, because nucleation is so facile, numerous phase interfaces are spontaneously formed in a direct coexistence simulation, and so direct coexistence simulations were not useful in phase diagram determination at this stage.

However, we have used direct coexistence simulations in certain cases as a check in confirming that the Frenkel–Ladd simulations yielded the correct coexistence points.

Thermodynamic integration

Thermodynamic integration [10, 11] refers to a series of integration schemes of thermodynamic potentials. For integration along iso- (βp) curves, where $\beta \equiv 1/k_B T$, we start from the product rule

$$\left(\frac{\partial(G/T)}{\partial T}\right)_{(\beta p)} = \frac{1}{T} \left(\frac{\partial G}{\partial T}\right)_{(\beta p)} - \frac{G}{T^2}, \quad (5)$$

from where an application of simple thermodynamics allows us to write

$$\left(\frac{\partial(G/T)}{\partial T}\right)_{(\beta p)} = -\frac{U}{T^2}. \quad (6)$$

This can be integrated to give

$$\frac{G_2}{Nk_B T_2} = \frac{G_1}{Nk_B T_1} - \int_{T_1}^{T_2} \frac{U}{Nk_B T^2} dT, \quad (7)$$

and this is the result we require for thermodynamic integration. Provided we know the Gibbs energy at some T_1 , then we can find the Gibbs energy at T_2 along the iso- (βp) curve by running several NpT simulations for temperatures between T_1 and T_2 (at fixed βp), and finding a polynomial fit to the integrand, which can then be integrated analytically. Analogous results arise for integration along isobars [10],

$$\frac{G_2}{Nk_B T_2} = \frac{G_1}{Nk_B T_1} - \int_{T_1}^{T_2} \frac{H}{Nk_B T^2} dT, \quad (8)$$

and isotherms [10],

$$\frac{A_2}{Nk_B T} = \frac{A_1}{Nk_B T} + \int_{\rho_1}^{\rho_2} \frac{p}{k_B T \rho^2} d\rho. \quad (9)$$

It is also possible to extend the scheme by coupling to a different hamiltonian, such that the potential energy is given by $U = U_{\text{real}} + \lambda U_{\text{extra}}$, and then integrating along λ ; we find that [10]

$$A(\lambda = 1) = A(\lambda = 0) + \int_0^1 \langle U_{\text{extra}} \rangle d\lambda. \quad (10)$$

This is known as hamiltonian thermodynamic integration [10] and is one component of the Einstein crystal Frenkel–Ladd approach [11].

The free energy of a fluid phase evaluated from the ideal gas by decreasing the pressure at constant temperature is given by [10]

$$\frac{A}{Nk_B T} = \ln(\rho \Lambda^3) - 1 + \int_0^{\rho} \left[\frac{p}{k_B T \rho^2} - \frac{1}{\rho} \right] d\rho, \quad (11)$$

where Λ is the de Broglie thermal wavelength. It is usually beneficial to fit the entire integrand to a single polynomial to avoid diverging terms. As the density tends to zero, the integrand tends to the second virial coefficient [10]; it is helpful to evaluate this explicitly to benchmark the simulation results.

Gibbs–Duhem integration

In Gibbs–Duhem integration [10, 24], we numerically integrate the Clapeyron equation,

$$\frac{dp}{dT} = \frac{\Delta H}{T \Delta V}, \quad (12)$$

or an analogous expression, in order to obtain new coexistence points from already known coexistence points. In our simulations, we used the fourth-order Runge–Kutta algorithm to perform this integration.

Frenkel–Ladd Einstein crystal approach

The Einstein crystal approach [10, 11] is a fairly involved way of calculating the free energy of a crystal from the Einstein crystal, for which the free energy is known. We direct the interested reader to Frenkel and Smit’s book (Ref. [30]) and the review paper by Vega and co-workers (Ref. [10]) for an in-depth discussion of the method. In the Frenkel–Ladd scheme as implemented for our model, we take the rotational energy to be

$$u_{\text{Ein, or, } i} = \Lambda_{\text{rot}} \sin^2 \left[\frac{p}{2} (\varphi_i - \varphi_{i, \text{orig}}) \right], \quad (13)$$

where Λ_{rot} is a constant that we vary and $p = 5$ is the number of patches. We thus ensure that the particle’s symmetry is accounted for: rotations into degenerate positions give the same Frenkel–Ladd energy.

Reliability of free energy calculations

Computing absolute free energies from simulations requires a combination of numerical techniques, each of which can introduce errors, both systematic and random. Since it is difficult to keep track of how the errors propagate, the approach which is usually undertaken is to perform *a posteriori* checks on the whole process. As discussed by Vega and co-workers [10], ‘consistency checks’ can be applied to simulations to ensure that the data obtained in free energy calculations are

self-consistent and correspond to reality. There are several such checks that can be performed. For example, we can calculate the free energy at a particular point using several routes (*e.g.* by integrating along different isotherms, isobars or iso- (βp) curves to the same point). Furthermore, direct coexistence simulations can be used to ensure that the transition temperature does in fact occur where free energy curves intersect. Finally, in simulations involving Gibbs–Duhem integration, we can integrate first in the ‘forward’ and then in the ‘reverse’ direction, ensuring that the method reproduces the starting point. We have performed all these checks to ensure that the results we have obtained are robust.

Gao and co-workers compared the results of Debye crystal reference state calculations with different force constants to obtain an estimate of the error in the free energy of hexagonal ice [33]. We do something similar to estimate the error in free energy in Fig. 2 in the main paper: we calculate the Frenkel–Ladd free energy at several points ($k_{\text{B}}T/\varepsilon = 0.1$, $k_{\text{B}}T/\varepsilon = 0.15$, $k_{\text{B}}T/\varepsilon = 0.17$ and $k_{\text{B}}T/\varepsilon = 0.19$) along the iso- (βp) curve, and then use thermodynamic integration to obtain free energies from each of the starting Frenkel–Ladd free energies. The largest difference in free energy between any pair of calculations along the entire curve can then serve as an estimate of the error in free energy in our simulations. The *largest* such deviation was $\Delta(\Delta g)/k_{\text{B}}T = 0.012$, which is sufficiently small not to affect any conclusion, and the error in practice is likely to be significantly smaller, as we were able to confirm phase transition temperatures in independent direct coexistence simulations.